

VISUALIZATION OF FLOW CHARACTERISTICS BETWEEN THE RIBBED PLATES VIA PARTICLE IMAGE VELOCIMETRY

by

Ilker GOKTEPELI*, **Ulas ATMACA**, and **Sercan YAGMUR**

Department of Mechanical Engineering, Faculty of Engineering and Natural Sciences,
Konya Technical University, Konya, Turkey

Original scientific paper
<https://doi.org/10.2298/TSCI180727300G>

Heat transfer is considerably influenced by flow stagnation, separation and reattachment regions due to the ribbed plates. Placing the ribs such as fins, turbulators that trigger the flow separation, enhances the heat transfer inside the channel by increasing the turbulence intensity. The flow separation is caused by disturbing the thermal and hydrodynamic development lengths. Moreover, these ribs also make an impact that increases the heat transfer by enlarging the heat transfer area. However, the ribs lead to the increment of the required pumping power in the meantime due to the increasing pressure loss in such systems. This aforementioned method is used for the heat exchangers, the solar collectors, the cooling of electronic devices. The investigation of the flow characteristics is very crucial to understand the heat transfer mechanism in the ducts for this reason. In the present paper, the flow characteristics between the plates have been experimentally researched. Particle image velocimetry system in the open water channel of Selcuk University Advanced Technology Research and Application Center has been used. The smooth plates have been taken as the reference model and used for the comparison with the plates having the rectangular cross-sectional ribs. The ribs with various heights of $0.1 \leq h' = h/H \leq 0.3$ have been symmetrically placed on the internal surfaces of the plates via several spacing values of $0.5 \leq S' = S/H \leq 1$ for varying Reynolds numbers as $10000 \leq Re \leq 20000$. As a result, the flow characteristics have been given in terms of the contour graphics for velocity vector field, velocity components and vorticity.

Key words: *flow separation, parallel plate, particle image velocimetry, Reynolds number, rib, turbulent flow*

Introduction

The artificial surface elements are utilized to enhance the convection heat transfer for the flow inside the ducts. This method is encountered in practice with a number of application fields. Heat exchangers, solar collectors, cooling parts of electronic devices, internal cooling passages of gas turbines, and also chemical processes are given as the examples for the aforementioned case.

It is known that heat transfer is particularly affected *via* flow stagnation, separation and reattachment regions between the ribbed plates. Placing the ribs such as the fins, the turbulators causing the flow separation and enlarging the heat transfer area, is very effective method

* Corresponding author, e-mail: igoktepe@ktun.edu.tr

for the heat transfer augmentation inside the ducts. The ribs placed between the parallel plates, cause the flow separation by disturbing the thermal and hydrodynamic development lengths and rotational flows in front of them. In the literature, this kind of flow is explained with the step flow which is the simplest shear flow where the flow that separates and reattaches. In general, the step flow is classified as in forward-facing step flow, Sherry *et al.* [1], cavity flow, Timuralp and Altac [2], and backward-facing step flow, Aung [3], Mushahet [4]. Each of these flows can occur separately and there are some situations where two or all of them can be observed for the same problem. It is possible to consider both the forward-facing step flow and the backward-facing step flow at the same time for the flow over a single rib. As in this study, the forward flow-facing step flow, the cavity flow and the backward-facing step flow are seen together for the flow over the ribs mounted periodically.

Different geometrical shapes for the ribs have been experimentally and/or numerically studied in the literature. Especially, the rectangular ribs are more common shape compared to the other geometrical shapes. The arrangement of the ribs affects the overall performance depending on the circumstances. For example, the effects of the rectangular cross-sectional ribs on heat transfer have been considered for the staggered arrangement, Mayle [5], Webb and Ramadhyani [6], Liu and Wang [7], Wongcharee *et al.* [8], Desrues *et al.* [9], Xie *et al.* [10], Marocco and Franco [11]. On the other hand, the rectangular ribs have also been investigated in terms of the symmetrical arrangement, Hwang and Liou [12], Lopez *et al.* [13], Tafti [14], Pourmahmoud *et al.* [15], Tokgoz *et al.* [16]. In some studies for the comparison, staggered and symmetrical arrangements have been given together for the rectangular cross-sectional ribs, Promvongse and Thianpong [17], Skullong *et al.* [18], Vanaki and Mohammed [19], Yang *et al.* [20]. In the literature, second common shape is the triangular cross-sectional ribs. Different orientations and arrangements have been seen in the studies including the triangle ribs. The staggered arrangement, Kilicaslan and Sarac [21], and the symmetrical arrangement, Pehlivan *et al.* [22], Aslan *et al.* [23], for the triangular cross-sectional ribs have been seen. Moreover, the specific geometrical shapes for the ribs have also been encountered such as convex-concave, Wongcharee *et al.* [8], Yemenici and Umur, [24], semi-circular cross-sectional, Kilicaslan and Sarac [21], Nine *et al.* [25], sinusoidal, Aslan *et al.* [23], diamond-shaped, Sripattanapipat and Promvongse [26], trapezoidal, Ahmed *et al.* [27], in the previous studies. However, the ribs lead to the increment of the required pumping power in the meantime due to the increasing pressure loss in such systems. For this reason, the examination of the flow characteristics is very important to understand the heat transfer mechanism in the parallel plates.

In the present study, the ribs with various heights of $0.1 \leq h' = h/H \leq 0.3$ have been symmetrically placed on the internal surfaces of the plates *via* several spacing values of $0.5 \leq S' = S/H \leq 1$ for varying Reynolds numbers as $10000 \leq Re \leq 20000$. The flow characteristics have been given in terms of the contour graphics for velocity vector field, velocity components and vorticity *via* particle image velocimetry (PIV) method.

Methodology

All experiments have been done in a large-scale open water channel of Selcuk University Advanced Technology Research and Application Center as shown in fig. 1. Flow characteristics have been experimentally studied for $Re = U_\infty D_H / \nu = 10000, 15000, \text{ and } 20000$ by considering the system capacity. In the study, U_∞ is the free-stream velocity, the hydraulic diameter is expressed as $D_H = 2H$, Dean [28], depending on the distance between the plates and ν is the kinematic viscosity.

The dimensions of the channel with the rectangular cross-section are $6 \times 0.77 \times 0.6$ m for length, width, and height, respectively. The glasses with low light refraction having the thickness of 15 mm have been used in the water channel to make the laser beam passing easier. The channel has been filled with water up to $h_w = 0.47$ m. Water is circulated in the channel *via* the centrifugal pump in terms of the closed loop and the speed value of the centrifugal pump is controlled by using a frequency converter.

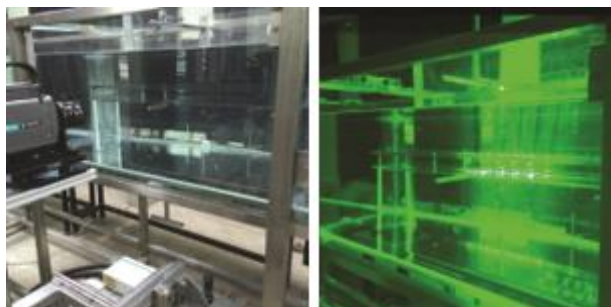


Figure 1. The experiments in the water channel

The re-circulation is provided between two water tanks which are large enough and the honeycomb filter is utilized for flow regulation. The Nd:YAG laser source with a maximum value of 15 Hz has been operated to obtain the laser sheet with the thickness of 1 mm. The silver-coated hollow particles with the spherical diameter of $10 \mu\text{m}$ have been used since there is no difference between the density values of particle and water. All images have been captured *via* a high speed complementary metal oxide semiconductor (CMOS) camera with the resolution of 1632×1200 pixels. Using the high speed digital camera, two digital photos in a row of the particles in the region enlightened by the laser beam, have been taken for the time interval, Δt , with the level of microsecond. Throughout the experiments, 1024 digital images have been attained after getting 1025 pairs of digital photos. In the software of the experimental set-up, all images have been divided into small interrogation areas with 32×32 pixels. Approximately 20-30 particles have been contained in each interrogation areas to provide the high-image density criterion. Since the Δt and the distance that the particles travel through the time interval are known, the velocity vectors have been calculated *via* the software. The raw vector maps obtained as a result of the calculation have been provided for each time step. However, erroneous velocity vectors can occur in the flow field owing to the laser reflections observed during the image capture. In terms of the post processing, the Dantec Dynamic Studio has been employed to attain the raw displacement vector fields from the experimental data by applying the appropriate filters embedded in the software.

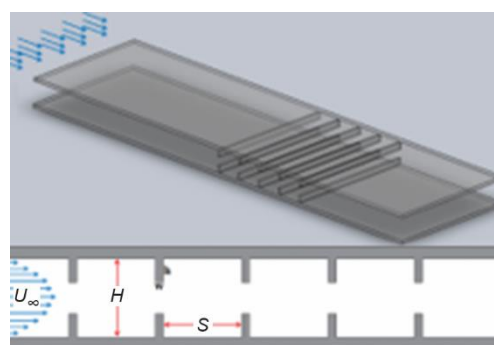


Figure 2. The schematic of the model used in the experiments

The material of the plates and the ribs has been chosen as plexiglass, a transparent material, in order to allow the laser beam to pass smoothly through the model during the experiments. The model has been positioned at the uniform flow conditions for the minimization of the effects of the free surface and the boundary-layer at the channel base. In order to keep the model at the desired position in the water channel and to be exposed to uniform flow conditions, the set-up has been designed. The flow characteristics have not been affected by the connectors. As given in fig. 2, the height of the duct is $H = 0.05$ m for the system. All dimensions have been normalized with the height as done, $L' = L/H = 20$, for the length of the channel. Also, the width of the plates has been given as $W' = W/H = 6$. The

thickness of each plate was 0.008 m, which is the lowest value to facilitate the laser transmission.

Six bolt-nut connections have been used to provide the distance between two parallel plates. The distance between the center of each bolt-nut connection and the nearest edge was 0.03 m and determined by taking into consideration that the connection apparatuses do not affect the flow conditions. The ribs have been bonded to the plates with the silicone adhesive after the point of $L' = 10$ that corresponds the fully developed flow region. The width of the rib is indicated as $w' = w/H = 0.1$ which has been kept constant for the present study. The height for the ribs varies from $h' = h/H = 0.1$ to 0.3 while the spacing between the ribs is from $S' = S/H = 0.5$ to 1. Ten models have been formed with respect to the aforementioned dimensions. All images have been captured for $9.5 \leq L' \leq 18.5$ in two stages by scanning this interval with the camera and laser system together.

Results and discussion

Flow characteristics between the parallel plates have been presented as a result of the experiments in the water channel *via* PIV method. The comparison of the smooth and the ribbed plates have been done in terms of time-averaged results for velocity vector field \vec{V} , streamwise velocity component \bar{u} , cross-stream velocity components \bar{v} , and vorticity $\bar{\omega}$ for Reynolds numbers of 10000, 15000, and 20000. All images have been given with respect to the formation below:

Velocity vector fields, \vec{V} , have been given for $Re = 10000$, 15000, and 20000 in fig. 3. For the smooth plate, there is no deterioration for the flow conditions since there is no rib in the channel. Therefore, uniform flow structure has been observed. For the ribbed plates, the cross-section area of the flow has been narrowed by increasing the rib height. As a result, the velocity vectors are more intense in this area. With the increasing rib height, the flow has begun to deteriorate further and the flow separation has been seen more clearly. The reverse flows have

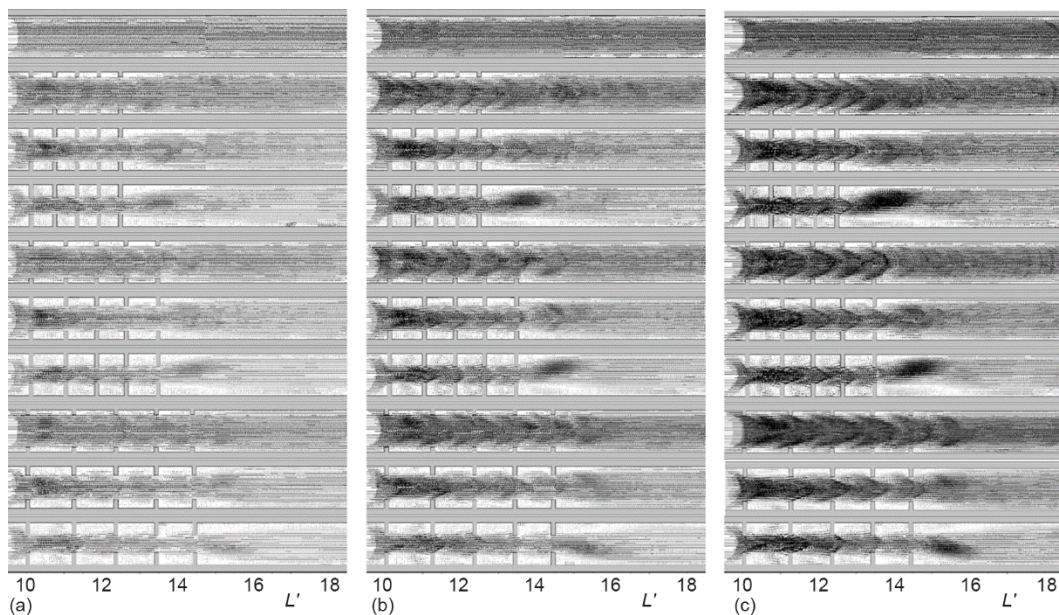


Figure 3. Velocity vector fields, \vec{V} , at (a) $Re = 10000$, (b) $Re = 15000$ and (c) $Re = 20000$

been observed with the resulting flow separations. In this case, there are the effects of the forward-facing step flow in the upstream direction of the first rib, the cavity flow between the two ribs and the backward-facing step flow in the wake region of the last ribs. The rotational flow between the first two ribs is stronger. Subsequently, this effect has been relatively reduced by the other ribs. In the formation of secondary flows between the ribs, the cavity flow is dominant. As the rib height has been increased, the symmetrical flow structure has been disturbed by the jet flow effect. In addition, when the spacing between the ribs has been enlarged, the region of the velocity vectors localization has extended along the distance towards the exit. As the turbulence intensity for the flow increased depending on the increase of Reynolds number, the velocity vectors have indicated a denser and more complex flow structure.

Streamwise velocity components, \bar{u} , have been presented for $Re = 10000$, 15000 , and 20000 in fig. 4. In case of the smooth plate, the maximum velocity value has been obtained as 10% greater of the fluid velocity entering to the system. Since there is no rib in the channel, no deterioration has been observed in the flow structure. The velocity values have decreased with the effect of the boundary-layer as a consequence of the no slip condition on the plate wall. In the ribbed models, increasing the rib height has narrowed the flow cross-sectional area. As a result, the velocity values in this region have increased. With the increasing rib height, the flow has been much disturbed due to the flow separation. With the effect of flow separation, reverse flows have been obtained. This effect has tended to increase due to the increasing rib height. In particular, the secondary flows were stronger in the region between the first two ribs. This is explained by the forward-facing step flow in the upstream direction of the first rib, the cavity flow between the two ribs and the backward-facing step flow in the wake of the last rib. This kind of flow is relatively ineffective between the other ribs when compared to the flow between the first two ones. As observed, the maximum values of the streamwise velocity components have been attained between the first two ribs. After that, periodical flow has been seen up to the last ribs. However, the region where maximum values attained has tended to shrink owing to the increase of Reynolds number and the rib height. This situation has been observed depending

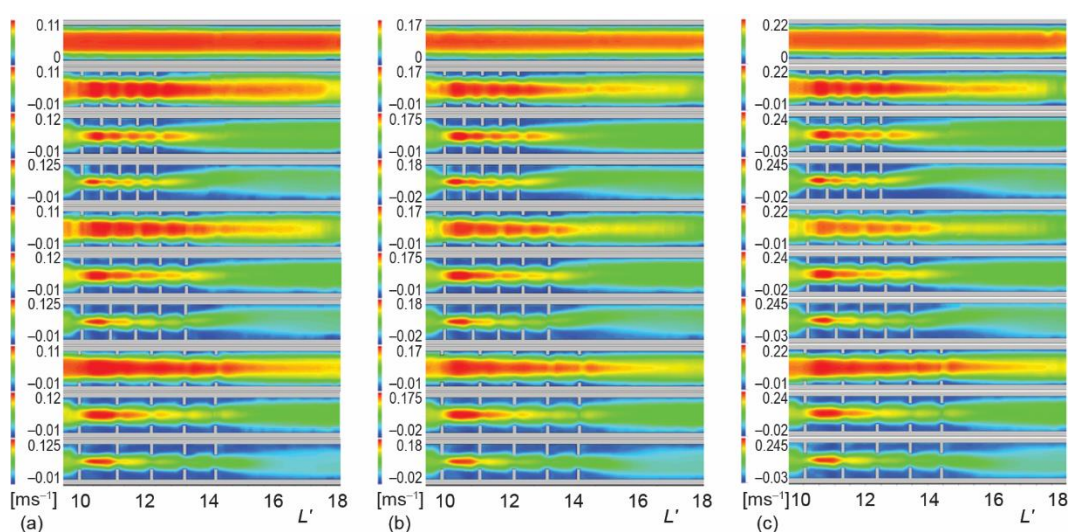


Figure 4. Streamwise velocity components \bar{u} , at (a) $Re = 10000$, (b) $Re = 15000$ and (c) $Re = 20000$
 (for color image see journal web site)

on the increasing fluctuations and laser reflections, respectively. Moreover, asymmetrical flow structure has been encountered as a result of the aforementioned circumstances. The change in the spacing between the ribs has less effect.

Cross-stream velocity components, \bar{v} , have been indicated for $Re = 10000$, 15000 , and 20000 in fig. 5. For the smooth plate, there is not much change for the cross-stream velocity components in the considered region of $9.5 \leq L' \leq 18.5$ since there is no rib mounted on the plates. The maximum and minimum values in the legend belong to the inlet of the duct. In case of the ribbed plates, there is almost symmetry for the flow structure. Complete symmetry has not been provided due to undesired laser reflection. Symmetrical flow conditions have been slightly broken down as a result of the increasing rib height. The upstream corner of the first rib has triggered the flow separation. For this reason, the maximum and the minimum values have been obtained at the mentioned corner for the models with the ribs. These values are negative for the ribs of the upper plates while the positive ones are on the lower ribbed plates. However, in case of the rib height of $h' = 0.1$, these clusters have not been observed at the upstream corner of the second ribs. With the increasing rib height, these clusters have begun to be visible with the reverse sign and the exact opposite has been seen for the first ribs. Because the velocity clusters with the minimum values have been observed for $h' = 0.1$ on the top plate and the maximum values have been attained on the bottom plate. In case of $h' = 0.2$, the velocity clusters have begun to be more visible. When the rib height is $h' = 0.3$, the signs of the velocity clusters and their dominancy regions have remained constant after the ribs. Furthermore, the clusters of the cross-stream velocity components have become evident by increasing the distance between the ribs. The influence of the rib spacing on the values of the cross-stream velocity components is nearly negligible; however, these values have been increased by ascending Reynolds numbers.

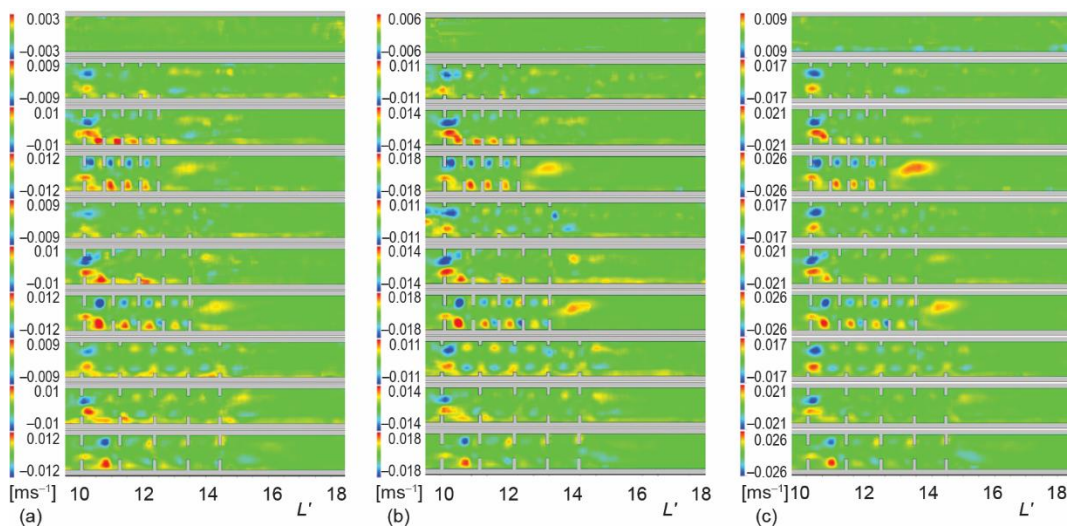


Figure 5. Cross-stream velocity components, \bar{v} , at (a) $Re = 10000$, (b) $Re = 15000$ and (c) $Re = 20000$ (for color image see journal web site)

Vorticity contours, $\bar{\omega}$, have been given for $Re = 10000$, 15000 , and 20000 in fig. 6. In case of the smooth plate, there is not much change for the vorticity contours in the considered

region of $9.5 \leq L' \leq 18.5$ since there is no rib mounted on the plates. The maximum and minimum values in the legend belong to the inlet of the duct. Almost symmetrical distribution has been observed in all cases with the ribs placed. The upstream corner of the first rib has greatly increased the flow separation. In all models where the ribs mounted, the maximum or the minimum values have been obtained at the corner of the first rib according to the position of the plate. The maximum values have been seen on the upper plate while the minimum values have been attained on the opposite plate. This situation has been explained by the direction of the vorticity rotation observed as a result of the flow separation. Although this situation is more effective between the first two ribs, the regional distribution of the vortices has shrunk between the other ribs in a row due to the periodical flow. However, the vortices occurring as a consequence of both the flow separation and the effect of the short-term periodical flow have elongated for the streamwise and shrunk for the cross-stream direction after the last rib. The elongation and the shrinkage have been clearly observed with the increasing Reynolds numbers. For all cases investigated, this effect has been seen just after the last rib for the distance of L' or $1.5 L'$ depending on the circumstances. The values of the vorticity have tended to increase with the ascending Reynolds numbers. On the other hand, the distance between two successive ribs has less effect on the vorticity contours. Since the effect is related to the flow separation, the rib height is more dominant.

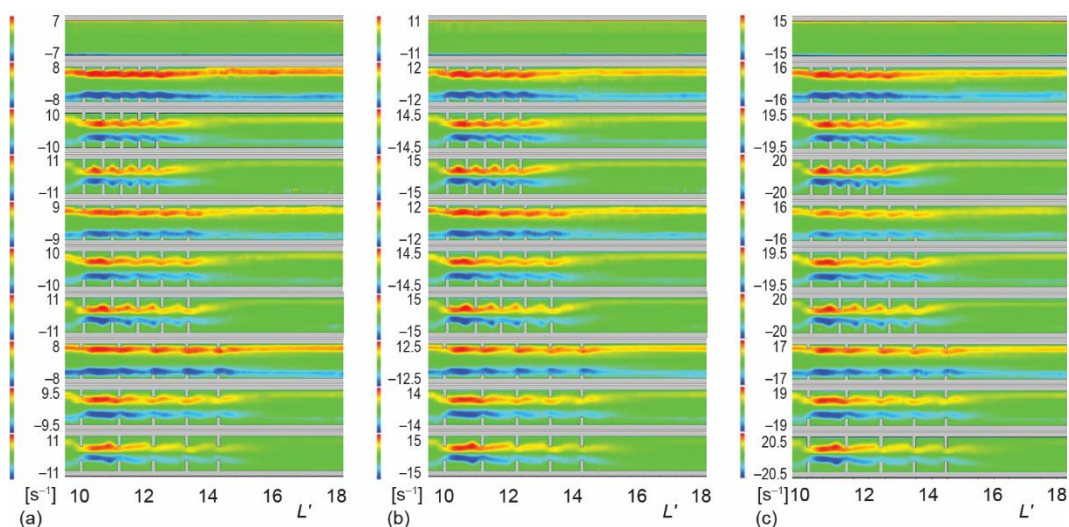


Figure 6. Vorticity contours, $\bar{\omega}$, at (a) $Re = 10000$, (b) $Re = 15000$ and (c) $Re = 20000$
 (for color image see journal web site)

Conclusions

The fluid flow characteristics between the horizontal parallel plates has been visualized by using PIV technique. Under the thumb of different rib heights, distances between the ribs and Reynolds numbers, the results obtained from the experiments can be outlined as follows.

- As expected, the flow structure has been disturbed with the ribs mounted on the plates.
- The rotational flow between the first two ribs is stronger.
- In the formation of secondary flows between the ribs, the cavity flow is dominant.

- As the rib height has been increased, the symmetrical flow structure has been disturbed by the jet flow effect.
- In the ribbed models, increasing the rib height has narrowed the flow cross-sectional area; as a result, the velocity values in this region have increased.
- The upstream corner of the first rib has triggered the flow separation.
- For all cases, the distance between the successive ribs has less effect on the flow characteristics.

Acknowledgment

This study has been supported by Selcuk University Academic Staff Training Program (OYP) with the project number of 2015-OYP-007.

The authors are thankful for Particle Image Velocimetry set-up established by Ministry of Development of the Republic of Turkey *via* the 2009K12180 coded project of Selcuk University Advanced Technology Research and Application Center.

Nomenclature

D_H – hydraulic diameter [m]

h – rib height [m]

H – distance between the plates [m]

L – length [m]

Re – Reynolds number ($= U_\infty D_H \nu^{-1}$)

S – spacing between the ribs [m]

U_∞ – free stream velocity [ms^{-1}]

\bar{u} – streamwise velocity component [ms^{-1}]

\vec{V} – velocity vector field

\bar{v} – cross-stream velocity component [ms^{-1}]

W – plate width [m]

w – rib width [m]

$\bar{\omega}$ – vorticity [s^{-1}]

w – water

' – dimensionless

Greek symbol

ν – kinematic viscosity [m^2s^{-1}]

Acronym

PIV – particle image velocimetry

CMOS – complementary metal oxide semiconductor

References

- [1] Sherry, M. J., Flow Separation Characterisation of a Forward Facing Step Immersed in a Turbulent Boundary Layer, *Proceedings, 6th International Symposium on Turbulence and Shear Flow Phenomena*, Seoul, South Korea, 2009, pp. 1325-1330
- [2] Timuralp, C., Altac, Z., Investigation of Combined Heat Transfer and Laminar Fluid Flow in Two and Three Dimensional Ducts with an Open Cavity, *Journal of Thermal Science and Technology*, 37 (2017), 2, pp. 33-47
- [3] Aung, W., An Experimental Study of Laminar Heat Transfer Downstream of Backsteps, *Journal of Heat Transfer*, 105 (1983), 4, pp. 823-829
- [4] Mushahet, K. S., Simulation of Turbulent Flow and Heat Transfer over a Backward-Facing Step with Ribs Turbulators, *Thermal Science*, 15 (2011), 1, pp. 245-255
- [5] Mayle, R. E., Pressure Loss and Heat Transfer in Channels Roughened on Two Opposed Walls, *Journal of Turbomachinery*, 113 (1991), 1, pp. 60-66
- [6] Webb, B., Ramadhyani, S., Conjugate Heat Transfer in a Channel with Staggered Ribs, *International Journal of Heat and Mass Transfer*, 28 (1985), 9, pp. 1679-1687
- [7] Liu, H., Wang, J., Numerical Investigation on Synthetical Performances of Fluid Flow and Heat Transfer of Semiattached Rib-Channels, *International Journal of Heat and Mass Transfer*, 54 (2011), 1-3, pp. 575-583
- [8] Wongcharee, K., et al., Numerical Investigation of Flow Friction and Heat Transfer in a Channel with Various Shaped Ribs Mounted on Two Opposite Ribbed Walls, *International Journal of Chemical Reactor Engineering*, 9 (2011), 1, A26
- [9] Desruets, T., et al., Numerical Prediction of Heat Transfer and Pressure Drop in Three-Dimensional Channels with Alternated Opposed Ribs, *Applied Thermal Engineering*, 45-46 (2012), Dec., pp. 52-63

- [10] Xie, G., et al., Computational Fluid Dynamics Modeling Flow Field and Side-Wall Heat Transfer in Rectangular Rib-Roughened Passage, *Journal of Energy Resources Technology*, 135 (2013), 4, ID 042001
- [11] Marocco, L., Franco, A., Direct Numerical Simulation and RANS Comparison of Turbulent Convective Heat Transfer in a Staggered Ribbed Channel with High Blockage, *Journal of Heat Transfer*, 139 (2017), 2, ID 021701
- [12] Hwang, J-J., Liou, T-M., Effect of Permeable Ribs on Heat Transfer and Friction in a Rectangular Channel, *Journal of Turbomachinery*, 117 (1995), 2, pp. 265-271
- [13] Lopez, J., et al., Heat Transfer in a Three-Dimensional Channel with Baffles, *Numerical Heat Transfer Part A Applications*, 30 (1996), 2, pp. 189-205
- [14] Tafti, D., Evaluating the Role of Subgrid Stress Modeling in a Ribbed Duct for the Internal Cooling of Turbine Blades, *International Journal of Heat and Fluid Flow*, 26 (2005), 1, pp. 92-104
- [15] Pourmahmoud, N., et al., The Effects of Longitudinal Ribs on Entropy Generation for Laminar Forced Convection in a Micro-Channel, *Thermal Science*, 20 (2016), 6, pp. 1963-1972
- [16] Tokgoz, N., et al., Investigation of Flow Characteristics and Heat Transfer Enhancement of Corrugated Duct Geometries, *Applied Thermal Engineering*, 118 (2017), May, pp. 518-530
- [17] Promvong, P., Thianpong, C., Thermal Performance Assessment of Turbulent Channel Flows over Different Shaped Ribs, *Int. Comm. in Heat and Mass Transfer*, 35 (2008), 10, pp. 1327-1334
- [18] Skullong, S., et al., Effects of Rib Size and Arrangement on Forced Convective Heat Transfer in a Solar Air Heater Channel, *Heat and Mass Transfer*, 51 (2015), 10, pp. 1475-1485
- [19] Vanaki, S. M., Mohammed, H., Numerical Study of Nanofluid Forced Convection Flow in Channels Using Different Shaped Transverse Ribs, *Int. Comm. in Heat and Mass Transfer*, 67 (2015), Oct., pp. 176-188
- [20] Yang, W., et al., Experimental Study on the Heat Transfer Characteristics of High Blockage Ribs Channel, *Experimental Thermal and Fluid Science*, 83 (2017), May, pp. 248-259
- [21] Kilicaslan, I., Sarac, H. I., Enhancement of Heat Transfer in Compact Heat Exchanger by Different Type of Rib with Holographic Interferometry, *Experimental Thermal and Fluid Science*, 17 (1998), 4, pp. 339-346
- [22] Pehlivan, H., et al., Experimental Study of Forced Convective Heat Transfer in a Different Arranged Corrugated Channel, *Int. Comm. in Heat and Mass Transfer*, 46 (2013), Aug., pp. 106-111
- [23] Aslan, E., et al., Finite Volume Simulation for Convective Heat Transfer in Wavy Channels, *Heat and Mass Transfer*, 52 (2016), 3, pp. 483-497
- [24] Yemenici, O., Umur, H., Experimental Aspects of Heat Transfer Enhancement over Various Flow Surfaces, *Heat Transfer Engineering*, 37 (2016), 5, pp. 435-442
- [25] Nine, M. J., et al., Turbulence and Pressure Drop Behaviors around Semicircular Ribs in a Rectangular Channel, *Thermal Science*, 18 (2014), 2, pp. 419-430
- [26] Sripattanapipat, S., Promvong, P., Numerical Analysis of Laminar Heat Transfer in a Channel with Diamond-Shaped Baffles, *Int. Comm. in Heat and Mass Transfer*, 36 (2009), 1, pp. 32-38
- [27] Ahmed, M., et al., Effects of Geometrical Parameters on the Flow and Heat Transfer Characteristics in Trapezoidal-Corrugated Channel Using Nanofluid, *Int. Comm. in Heat and Mass Transfer*, 42 (2013), Mar., pp. 69-74
- [28] Dean, R., Reynolds Number Dependence of Skin Friction and Other Bulk Flow Variables in Two-Dimensional Rectangular Duct Flow, *Journal of Fluids Engineering*, 100 (1978), 2, pp. 215-22